Quantum confinement effects in semiconductor clusters

M. V. Rama Krishna and R. A. Friesner
The Department of Chemistry, Columbia University, New York, New York 10027-6948

(Received 8 April 1991; accepted 15 August 1991)

The band gaps, band structure, and excited-state (exciton) energies of CdS, GaAs, and GaP semiconductor clusters are calculated using pseudopotentials. In addition, the sensitivity of the exciton energies to the size, shape, crystal structure, and lattice constant of the unit cell are investigated. The calculated exciton energies of CdS clusters are in excellent agreement with experiment over a wide range of cluster sizes. Also, the exciton states of small CdS clusters are sensitive to whether their crystal structure is zinc blende or hexagonal. Such a sensitivity is absent in large CdS clusters. Furthermore, small GaAs clusters are shown to exhibit anomalous redshift of their absorption spectra, in sharp contrast to CdS and large GaAs clusters whose spectra always shift to blue with decreasing cluster size. Finally, the lowest-energy non-Franck–Condon transition in GaP clusters always shifts to blue with decreasing cluster size, whereas the higher-energy Franck–Condon transition in small clusters exhibits the anomalous redshift. These novel findings reveal that (1) the optical spectroscopy of semiconductor clusters is strongly material and crystal structure dependent; (2) the spectroscopy of small clusters is dramatically different from those of large clusters and bulk; and (3) these effects cannot be explained, even qualitatively, using the effective-mass approximation.

I. INTRODUCTION

The onset of absorption of light by semiconductor materials is accompanied by the creation of a bound electron–hole pair called an exciton. For more than a decade scientists have been attempting to understand how the properties of this exciton are modified in semiconductor materials with reduced dimensionality, such as two-dimensional films and three-dimensional clusters.[1] In the case of clusters, the absorption threshold is observed to blueshift by up to 1 eV or more as the cluster size is decreased. Because of this large blueshift, clusters of different sizes exhibit different colors. We explain and for the first time quantitatively estimate the absorption threshold of CdS clusters, in excellent agreement with experiment. Furthermore, we predict that the spectra of small CdS clusters are sensitive to the crystal structure even though such a sensitivity is absent in large clusters. We also show that the physical shape and lattice relaxation significantly affect the absorption threshold in small clusters. Finally, we predict that the direct transitions in the absorption spectra of small GaAs and GaP clusters shift to the red instead of to the blue, with decreasing cluster size. All these findings provide insights into the exciton states in clusters, and will be helpful in the selection and synthesis of new materials with desired optical properties.

Semiconductor materials are characterized by a small but nonzero band gap. This band gap is larger in clusters. Consequently, the first absorption peak, corresponding to the threshold for the absorption of light, is normally shifted to the blue with decreasing cluster size. Although the basic principles governing the relationship between cluster size and the band gap appeared to be understood for some time, theoretical calculations have not been able to predict quantitatively the observed blueshift. The effect of other factors, such as the physical shape and crystal structure, has not been investigated. The adequacy of the effective-mass model (EMM), which is often used to explain the quantum confinement effects (QCE) in clusters, is unclear. Such a detailed understanding is necessary for a systematic search for materials with sought after structural, optical, electric, and magnetic properties. Together with the corresponding investigations of metal[2] and van der Waals clusters,[3] these studies will also provide insights into the origins of various macroscopic properties of matter.[4,5]

The first experimental evidence of QCE in clusters came from crystalline CuCl clusters grown in silicate glasses.[6] The silicate glasses, which initially contained compounds of Cu and Cl at $\approx 1\%$ concentration, were heated at constant temperature for a finite time to form CuCl clusters. The average size of the clusters could be controlled by the temperature and duration of the heat treatment. Spectroscopic studies on these clusters clearly indicated up to 0.1 eV blueshift of the absorption spectrum relative to that for the bulk. Theoretical analysis of the observed blueshift followed shortly thereafter, utilizing particle in a sphere[6] and effective-mass models.[7] At about the same time, Brus and co-workers developed a chemical method of synthesizing small clusters in colloidal suspensions, by kinetically controlling chemical reactions in the liquid phase.[8,9] This technique gave better control on the sizes and the composition of the clusters. Brus and co-workers thus heralded the era of controlled synthesis of clusters of definite size and composition. Equally important, Brus also gave a very detailed and elegant analysis of QCE on ionization potentials, electron affinities, redox potentials, and the absorption spectra.[10,11] He retained the effective-mass approximation for the kinetic energy of the electron–hole pair and used classical electrostatics to determine the potential energy of interaction of the electron and the hole with each other and with the surface. The early calculations of Brus and co-workers, based on this model, have yielded

the blueshift of the absorption spectrum in reasonable agreement with experiment for large clusters.[10]

The appealing simplicity of the theoretical analysis of Brus and its success in explaining the experimental data of that time, gave rise to considerable excitement in cluster science.[9,12–22] Here, we present a method that goes beyond the EMM and explains the experimental data of small clusters.

This paper is organized as follows. We first discuss the effective-mass model and its limitations in Sec. II and then present the theory of the empirical pseudopotential method in Sec. III. The details of our band-structure calculations are given in Sec. IV and the results of these calculations on CdS, GaAs, and GaP clusters are presented in Sec. V. In Sec. VI we review previous theoretical efforts aimed at understanding QCE in semiconductor clusters, and finally we conclude this paper with a brief summary in Sec. VII.

II. EFFECTIVE-MASS MODEL

The absorption of light by a semiconductor crystal results in the removal of an electron from the top of the valence band and the placement of the same electron at the bottom of the conduction band. Using the techniques of quantum-field theory, one may replace this interacting many-body quantum problem by a two-body problem consisting of an electron in the conduction band and a hole (absence of an electron) in the valence band.[23] The electron and the hole interact with the lattice, as well as with each other. To a good approximation the wave functions of the electron and hole are plane waves with masses m_e and m_h, respectively, in units of the free-electron mass m_0. The effect of the interaction of the electron and hole with the periodic potential of the lattice is such that m_e and m_h are usually less than m_0. In other words, the effect of the periodic potential on the electrons is subsumed in their effective masses. This is the effective-mass model. Brus and others have adopted this model for clusters also, except that the allowed wave vectors are assumed to be determined by the physical dimensions of the cluster.[9] If we model the cluster as a sphere, then the allowed wave vectors of the lowest exciton state are given by $\mathbf{k} = \pi/R$ and the EMM gives the exciton energy as[9,17]

$$E_x = E_g(\text{bulk}) + \frac{\hbar^2\pi^2}{2R^2}\left(\frac{1}{m_e}+\frac{1}{m_h}\right) - \frac{1.786}{\epsilon R} - 0.248E_{Ry}, \tag{1}$$

where E_g(bulk) is the bulk crystal band gap, R is the radius of the cluster, ϵ is the dielectric constant, and $E_{Ry} = \mu e^4/2\epsilon^2\hbar^2$ is the effective Rydberg energy of the exciton, μ being the reduced mass of the electron–hole pair.[17] The second, third, and fourth terms in Eq. (1) give kinetic (T), Coulomb (V_C), and correlation (E_c) energies of the electron–hole pair, respectively, in atomic units.

There are two major deficiencies of the EMM: (a) First, the effective masses are assumed to be independent of $\mathbf{k}$. Since the band structures in real materials usually deviate from the free-electron parabolic form for large $\mathbf{k}$, this assumption introduces significant errors into the calculations of small clusters. This approximation is particularly flawed in small band-gap materials, because deviations from the parabolic form are much more severe in these cases. (b) Second, since the periodic potential of the crystal determines the effective masses, if the lattice structure in small clusters is different from that in bulk then their effective masses will also be different. It is not possible to incorporate the effect of modified lattice structure of clusters into the EMM. These two deficiencies of the EMM turn out to be the primary reasons for the failure of this model to quantitatively predict the spectral shift of the absorption spectra of small clusters.

Since there is no systematic procedure to remedy the failings of the EMM, a microscopic approach is needed to understand the electronic structure of these clusters. Below we present such an alternative approach that appears to be quite powerful.

III. EMPIRICAL PSEUDOPOTENTIAL METHOD

The energies of the electronic states in a crystal or cluster are determined by the Schrödinger equation

$$H\psi_{n,\mathbf{k}}(\mathbf{r}) = E_n(\mathbf{k})\psi_{n,\mathbf{k}}(\mathbf{r}), \tag{2}$$

where H is the Hamiltonian, $\psi_{n,\mathbf{k}}$ are its wave functions, $E_{n,\mathbf{k}}$ are the corresponding eigenvalues, $\mathbf{k}$ are the wave-vector quantum numbers of the wave functions, and n are the band indices. It is impossible to solve this equation exactly for the large clusters of interest, which typically contain thousands of electrons. Consequently, several approximations are made to formulate this many-body problem into a numerically tractable form. First, the electrons in the inner orbits are assigned to the nuclei to obtain charged cores. Second, the Born–Oppenheimer approximation is imposed to clamp the cores to fixed lattice sites. Third, each valence electron is assumed to move independently in the mean field of the fixed cores and other valence electrons. With these approximations the exact crystal-field potential experienced by the valence electrons is replaced by an effective potential (pseudopotential) $V_p(\mathbf{r})$ to obtain the valence-electron Hamiltonian

$$H = -\frac{\hbar^2}{2m}\nabla^2 + V_p(\mathbf{r}). \tag{3}$$

There are numerous techniques for determining these pseudopotentials. Among these, the empirical pseudopotential method (EPM) has proved to be an elegant and simple means of obtaining the electronic energy levels (band structures or dispersion curves) of semiconductor crystals with reasonable accuracy.[24,25] We use this method in our studies of the clusters.

Since $V_p(\mathbf{r})$ has contributions from all the atoms in the crystal, it is given by

$$V_p(\mathbf{r}) = \sum_{\mathbf{R}j} v_j(\mathbf{r}-\mathbf{R}-\mathbf{d}_j), \tag{4}$$

where v_j is the atomic pseudopotential of the jth basis atom at a lattice site $\mathbf{R}$, $\mathbf{d}_j$ is the position vector of the jth basis atom relative to $\mathbf{R}$, and the summation is over all lattice sites and all the basis atoms j at each lattice site. The atomic potentials v_j may now be expanded as

$$v_j(\mathbf{r}-\mathbf{R}-\mathbf{d}_j)=\frac{1}{Nn_a}\sum_{\mathbf{G}} v_j(\mathbf{G})\exp[i\mathbf{G}\cdot(\mathbf{r}-\mathbf{R}-\mathbf{d}_j)], \tag{5}$$

where $\mathbf{G}$ are the reciprocal-lattice vectors, N are the number of lattice sites in the sample, and n_a are the number of basis atoms at each lattice site. With this definition, the form factors $v_j(\mathbf{G})$ are given by

$$v_j(\mathbf{G})=\frac{n_a}{\Omega_0}\int_V d\mathbf{r}\, v_j(\mathbf{r})\exp(-i\mathbf{G}\cdot\mathbf{r}), \tag{6}$$

where Ω_0 is the volume of the unit cell and

$$v_j^*(\mathbf{G})=v_j(-\mathbf{G}). \tag{7}$$

Furthermore, if $v_j(\mathbf{r})=v_j(|\mathbf{r}|)$, then Eq. (6) yields

$$v_j(\mathbf{G})=\frac{4\pi n_a}{\Omega_0}\int_V dr\, r^2 j_0(Gr)v_j(r) \tag{8}$$

$$=v_j(|\mathbf{G}|), \tag{9}$$

where j_l is the spherical Bessel function of order l. In other words, for spherically symmetric atomic pseudopotentials, the form factors depend only on the magnitude of the reciprocal-lattice vectors $\mathbf{G}$.

Substituting Eq. (5) into (4), we obtain

$$V_p(\mathbf{r})=\frac{1}{Nn_a}\sum_{\mathbf{G}}\sum_{\mathbf{R},j} v_j(\mathbf{G})\exp[i\mathbf{G}\cdot(\mathbf{r}-\mathbf{R}-\mathbf{d}_j)]. \tag{10}$$

The summations over $\mathbf{R}$ and j in Eq. (10) can be explicitly evaluated for different crystal structures to obtain closed-form expressions of $V_p(\mathbf{r})$ in terms of the pseudopotential form factors $v_j(\mathbf{G})$. For spherically symmetric atomic potentials, Eq. (9) considerably reduces the number of form factors needed to represent the pseudopotential $V_p(\mathbf{r})$. In the EPM, these form factors are the adjustable parameters to be determined by fitting them to the experimental optical data. The pseudopotential $V_p(\mathbf{r})$ thus obtained is then used in Eqs. (2) and (3) to obtain the energy levels of the valence electron. This procedure has given satisfactory band structures for a variety of semiconductor crystals.[24,25]

A. Pseudopotentials of diamond structure crystals

The diamond structure consists of two interpenetrating fcc lattices, displaced from each other along the body diagonal by $a_0/4$, a_0 being the lattice constant of the unit cell. Equivalently, we may view the diamond lattice as an fcc lattice with two identical basis atoms at each lattice site. For this case, $n_a=2$, $v_1(\mathbf{G})=v_2(\mathbf{G})$, and $\mathbf{d}_1=-\mathbf{d}_2=-\mathbf{t}_1$ if we take the origin of the coordinate system at $\mathbf{t}_1=(t_{1x},t_{1y},t_{1z})=(1,1,1)a_0/8$. Consequently, Eq. (10) gives[24,25]

$$V_p(\mathbf{r})=\sum_{\mathbf{G}} v_1(\mathbf{G})\left[\frac{1}{N}\sum_{\mathbf{R}}\exp(-i\mathbf{G}\cdot\mathbf{R})\right]\times\left[\frac{1}{n_a}\sum_j\exp(-i\mathbf{G}\cdot\mathbf{d}_j)\right]\exp(i\mathbf{G}\cdot\mathbf{r}) \tag{11}$$

$$=\sum_{\mathbf{G}} v_1(\mathbf{G})S(\mathbf{G})\exp(i\mathbf{G}\cdot\mathbf{r}) \tag{12}$$

if we define the structure function $S(\mathbf{G})$ as

$$S(\mathbf{G})=\frac{1}{n_a}\sum_j\exp(-i\mathbf{G}\cdot\mathbf{d}_j) \tag{13}$$

$$=\cos(\mathbf{G}\cdot\mathbf{t}_1) \tag{14}$$

and use the identity $\exp(-i\mathbf{G}\cdot\mathbf{R})=1$.

B. Pseudopotentials of zinc-blende structure crystals

The zinc-blende (or sphalerite) crystal structure is identical to diamond structure, except that the two basis atoms at each lattice site are different. For this case, $n_a=2$, $v_1(\mathbf{G})\neq v_2(\mathbf{G})$, and a simple extension of the above procedure for this structure, starting from Eq. (10), yields[25]

$$V_p(\mathbf{r})=\sum_{\mathbf{G}}\left[\frac{1}{n_a}\sum_j v_j(\mathbf{G})\exp(-i\mathbf{G}\cdot\mathbf{d}_j)\right]\exp(i\mathbf{G}\cdot\mathbf{r}) \tag{15}$$

$$=\sum_{\mathbf{G}}\{\tfrac{1}{2}[v_1(\mathbf{G})\exp(i\mathbf{G}\cdot\mathbf{t}_1)+v_2(\mathbf{G})\exp(-i\mathbf{G}\cdot\mathbf{t}_1)]\}\times\exp(i\mathbf{G}\cdot\mathbf{r}) \tag{16}$$

$$=\sum_{\mathbf{G}}[V_s(G)S_S(\mathbf{G})+iV_A(G)S_A(\mathbf{G})]\exp(i\mathbf{G}\cdot\mathbf{r}), \tag{17}$$

where the symmetric (V_S) and antisymmetric (V_A) form factors are given by

$$V_S(G)=\tfrac{1}{2}[v_1(G)+v_2(G)],\qquad V_A(G)=\tfrac{1}{2}[v_1(G)-v_2(G)], \tag{18}$$

and the symmetric (S_S) and antisymmetric (S_A) structure factors are given by

$$S_S(\mathbf{G})=\cos(\mathbf{G}\cdot\mathbf{t}_1),\quad S_A(\mathbf{G})=\sin(\mathbf{G}\cdot\mathbf{t}_1). \tag{19}$$

If we define the reciprocal-lattice vectors $\mathbf{G}$ as

$$\mathbf{G}=\frac{2\pi}{a_0}(G_x,G_y,G_z), \tag{20}$$

and substitute it into (19), we obtain

$$S_S(\mathbf{G})=\cos\left[\frac{\pi}{4}(G_x+G_y+G_z)\right],\qquad S_A(\mathbf{G})=\sin\left[\frac{\pi}{4}(G_x+G_y+G_z)\right]. \tag{21}$$

C. Pseudopotentials of hexagonal structure crystals

The hexagonal (or wurtzite) crystal structure is similar to that of zinc blende, except that there are four basis atoms of two different types at each lattice site. For this case, $n_a=4$ and starting from Eq. (15), we obtain

$$V_p(\mathbf{r})=\sum_{\mathbf{G}}\frac{1}{n_a}\{v_1(\mathbf{G})[\exp(-i\mathbf{G}\cdot\mathbf{d}_1)+\exp(-i\mathbf{G}\cdot\mathbf{d}_3)]+v_2(\mathbf{G})[\exp(-i\mathbf{G}\cdot\mathbf{d}_2)+\exp(-i\mathbf{G}\cdot\mathbf{d}_4)]\}\times\exp(i\mathbf{G}\cdot\mathbf{r}), \tag{22}$$

since atoms 1 and 3, and 2 and 4 are identical in the hexagonal lattice. Rewriting v_1 and v_2 in terms of V_S and V_A using Eq. (18), and substituting these into the above equation, we obtain Eq. (17) with the structure functions defined as

$$S_S(\mathbf{G}) = \frac{1}{n_a}\sum_j \exp(-i\mathbf{G}\cdot\mathbf{d}_j),$$
$$S_A(\mathbf{G}) = \frac{-i}{n_a}\sum_j P_j \exp(-i\mathbf{G}\cdot\mathbf{d}_j), \tag{23}$$

where $P_j = +1$ when $j = 1,3$ and $P_j = -1$ when $j = 2,4$. Thus the pseudopotentials of hexagonal and zinc-blende crystals differ from each other only in the definition of the structure factors. We can carry out the summations in Eq. (23) as shown below.

The hexagonal lattice is characterized by three parameters: a_0, c_0, and u_0. Like zinc blende, the hexagonal lattice has tetrahedral coordination about each ion, but the orientation of the tetrahedron is different from that of zinc blende.[26] If we assume perfect tetrahedral coordination, then[27]

$$c_0/a_0 = \sqrt{8/3}, \quad u_0 = 0.375. \tag{24}$$

The direct lattice primitive translation vectors of the hexagonal lattice are

$$a_1 = \left(\frac{\sqrt{3}}{2}, -\frac{1}{2}, 0\right)a_0,$$
$$a_2 = (0,1,0)a_0, \tag{25}$$
$$a_3 = \left(0,0,\frac{c_0}{a_0}\right)a_0,$$

and the position vectors of the basis atoms are

$$d_1 = (-\tfrac{1}{6}a_1, -\tfrac{1}{6}a_2, -\tfrac{1}{4}(1-2u_0)a_3),$$
$$d_2 = (-\tfrac{1}{6}a_1, -\tfrac{1}{6}a_2, -\tfrac{1}{4}(1+2u_0)a_3),$$
$$d_3 = (\tfrac{1}{6}a_1, \tfrac{1}{6}a_2, \tfrac{1}{4}(1-2u_0)a_3), \tag{26}$$
$$d_4 = (\tfrac{1}{6}a_1, \tfrac{1}{6}a_2, \tfrac{1}{4}(1+2u_0)a_3).$$

Substituting Eq. (25) into (26), we obtain

$$d_1 = \left(-\frac{1}{4\sqrt{3}}, -\frac{1}{12}, -\frac{1-2u_0}{\sqrt{6}}\right)a_0,$$
$$d_2 = \left(-\frac{1}{4\sqrt{3}}, -\frac{1}{12}, -\frac{1+2u_0}{\sqrt{6}}\right)a_0,$$
$$d_3 = \left(\frac{1}{4\sqrt{3}}, \frac{1}{12}, \frac{1-2u_0}{\sqrt{6}}\right)a_0, \tag{27}$$
$$d_4 = \left(\frac{1}{4\sqrt{3}}, \frac{1}{12}, \frac{1+2u_0}{\sqrt{6}}\right)a_0,$$

in Cartesian coordinate representation.

In the zinc-blende crystal the nearest-neighbor atoms are located halfway along the face diagonal of the fcc lattice. Consequently, if $a_0(\mathrm{ZB})$ is the lattice constant of the zinc-blende crystal, then the nearest-neighbor distance is

$$r_n(\mathrm{ZB}) = \frac{1}{\sqrt{2}}a_0(\mathrm{ZB}). \tag{28}$$

In the hexagonal crystal, the nearest-neighbor atoms are located along the hexagon. Consequently,

$$r_n(\mathrm{hex}) = a_0(\mathrm{hex}). \tag{29}$$

Since $r_n(\mathrm{ZB}) = r_n(\mathrm{hex})$, comparing Eqs. (28) and (29), we obtain the relation

$$a_0(\mathrm{ZB}) = \sqrt{2}a_0(\mathrm{hex}). \tag{30}$$

If we now substitute this equation into Eq. (20), we obtain

$$\mathbf{G} = \frac{\sqrt{2}\pi}{a_0(\mathrm{hex})}(G_x, G_y, G_z). \tag{31}$$

This definition allows the comparison of $\mathbf{G}$ vectors of zinc-blende and hexagonal crystals on an equal footing. Substituting Eqs. (27) and (31) into (23) and carrying out some algebraic manipulations, we obtain

$$S_S(\mathbf{G}) = \cos(\sqrt{2}\pi\mathbf{G}\cdot\mathbf{t}_2)\cos(2\pi u_0 G_z/\sqrt{3}),$$
$$S_A(\mathbf{G}) = \cos(\sqrt{2}\pi\mathbf{G}\cdot\mathbf{t}_2)\sin(2\pi u_0 G_z/\sqrt{3}), \tag{32}$$

where $\mathbf{t}_2 = (1/\sqrt{48}, 1/12, 1/\sqrt{6})$.

We can also define $\mathbf{G}$ as

$$\mathbf{G} = (lb_1, mb_2, nb_3), \tag{33}$$

where b_1, b_2, and b_3 are the reciprocal-lattice primitive translational vectors given by

$$b_1 = \frac{\sqrt{2}\pi}{a_0}(\sqrt{8/3}, 0, 0),$$
$$b_2 = \frac{\sqrt{2}\pi}{a_0}(\sqrt{2/3}, \sqrt{2}, 0), \tag{34}$$
$$b_3 = \frac{\sqrt{2}\pi}{a_0}(0, 0, \sqrt{2}a_0/c_0).$$

Substituting Eqs. (26) and (33) into (23), utilizing the relations

$$b_i\cdot a_i = 2\pi, \quad b_i\cdot a_j = 0 \quad (i \neq j), \tag{35}$$

and carrying out some algebraic manipulations, we will obtain[25]

$$S_S(\mathbf{G}) = \cos\left[2\pi\left(\frac{l}{6}+\frac{m}{6}+\frac{n}{4}\right)\right]\cos(\pi n u_0),$$
$$S_A(\mathbf{G}) = \cos\left[2\pi\left(\frac{l}{6}+\frac{m}{6}+\frac{n}{4}\right)\right]\sin(\pi n u_0). \tag{36}$$

Equations (32) and (36) are equivalent. We have used both these equations in our calculations of hexagonal CdS and obtained identical results.

IV. BAND-STRUCTURE CALCULATIONS

A. Bulk crystals

To obtain the energy levels of the valence electron, we first expand its wave function as

$$\psi_{n,\mathbf{k}}(\mathbf{r}) = \frac{1}{\sqrt{V}}\sum_{\mathbf{G}} a_{n,\mathbf{k}}(\mathbf{G})\exp[i(\mathbf{G}+\mathbf{k})\cdot\mathbf{r}]. \tag{37}$$

Subsequently, we multiply Eq. (2) from the left by $\psi^*_{n,\mathbf{k}}$, substitute Eq. (37) for $\psi_{n,\mathbf{k}}$, and integrate over all volume, to obtain

$$\sum_{\mathbf{G}'} a_{n,\mathbf{k}}(\mathbf{G}')\sum_{\mathbf{G}}[H(\mathbf{G}'+\mathbf{k},\mathbf{G}+\mathbf{k}) - E_{n,\mathbf{k}}\delta_{\mathbf{G}'\mathbf{G}}]a_{n,\mathbf{k}}(\mathbf{G}) = 0. \tag{38}$$

This gives a set of secular equations

$$\sum_{\mathbf{G}} [H(\mathbf{G}'+\mathbf{k},\mathbf{G}+\mathbf{k}) - E_{n,\mathbf{k}}\delta_{\mathbf{G}'\mathbf{G}}]a_{n,\mathbf{k}}(\mathbf{G}) = 0, \quad (39)$$

where

$$H(\mathbf{G}'+\mathbf{k},\mathbf{G}+\mathbf{k}) = \frac{1}{V}\int d\mathbf{r}\exp[-i(\mathbf{G}'+\mathbf{k})\cdot\mathbf{r}] \times H\exp[i(\mathbf{G}+\mathbf{k})\cdot\mathbf{r}] \quad (40)$$

$$= \frac{\hbar^2}{2m}(\mathbf{G}+\mathbf{k})^2\delta_{\mathbf{G}'\mathbf{G}} + V(\mathbf{G}'-\mathbf{G}) \quad (41)$$

are the matrix elements of the Hamiltonian in the plane wave $\exp[i(\mathbf{G}+\mathbf{k})\cdot\mathbf{r}]/\sqrt{V}$ basis.

For diamond structure crystals, these matrix elements are given by

$$H_{\mathbf{G}\mathbf{G}'}(\mathbf{k}) = \frac{\hbar^2}{2m}(\mathbf{G}+\mathbf{k})^2\delta_{\mathbf{G}\mathbf{G}'} + v_1(|\mathbf{G}-\mathbf{G}'|)S(\mathbf{G}-\mathbf{G}'). \quad (42)$$

On the other hand, for zinc-blende and hexagonal crystal structures, these same matrix elements are given by

$$H_{\mathbf{G}\mathbf{G}'}(\mathbf{k}) = \frac{\hbar^2}{2m}(\mathbf{G}+\mathbf{k})^2\delta_{\mathbf{G}\mathbf{G}'} + V_S(|\mathbf{G}-\mathbf{G}'|)S_S(\mathbf{G}-\mathbf{G}') + iV_A(|\mathbf{G}-\mathbf{G}'|)S_A(\mathbf{G}-\mathbf{G}'). \quad (43)$$

For bulk crystals, $\mathbf{k}$ is a continuously variable quantum number and the energy levels $E_{n,\mathbf{k}}$ form bands. To obtain these bands the eigenvalues as a function of $\mathbf{k}$ are calculated by repeated diagonalization of $H(\mathbf{k})$.

B. Clusters

The energy levels in clusters do not form bands. However, we may define the band structure in clusters as the collection of all discrete energy levels in the first Brillouin zone. One can obtain these energy levels from band-structure calculations by imposing appropriate boundary conditions on the wave functions. For example, suppose that the physical dimensions of a crystal are reduced from all sides to give a rectangular cluster with side lengths L_1, L_2, and L_3. The energy levels no longer form a continuum now; instead we obtain quantized energy levels with wave vectors

$$\mathbf{k} = \pi\left(\frac{n_x}{L_1},\frac{n_y}{L_2},\frac{n_z}{L_3}\right), \quad (44)$$

where n_x, n_y, and n_z are the quantum numbers of a particle in a box with infinite potentials at the boundaries. For the low-energy excitations under consideration, the assumption of infinite potentials at the boundaries is a good approximation. For the special case of a cubic cluster, $L_1 = L_2 = L_3 = L$, we obtain

$$\mathbf{k} = \frac{\pi}{L}(n_x,n_y,n_z). \quad (45)$$

We can now carry out the band-structure calculations at these allowed $\mathbf{k}$ states to obtain the energy levels of the clusters.

Similarly, if we model the cluster as a spherical object of radius R, the energy levels of the valence electrons will be quantized because of the spherical boundary. The wave vectors of the lowest allowed states are given by $j_0(k_nR) = 0$, whose solution is $\mathbf{k}_n = n\pi/R$.[28] Since $\mathbf{k}_n$ is along the radial direction, we project it onto each of the Cartesian axes with equal magnitude to obtain Cartesian components of $\mathbf{k}$. This procedure yields

$$\mathbf{k} = \frac{\pi}{\sqrt{3}R}(n_x,n_y,n_z). \quad (46)$$

These simple models of a cluster give an adequate understanding of the effect of quantum confinement on the electronic structure of the cluster.

C. Computational details

The clusters of interest in this paper have either zinc-blende or hexagonal lattice structures.[9,15,25,26] Consequently, the Hamiltonian matrices are complex valued Hermitian matrices. We diagonalized these matrices using the EISPACK routines CH, HTRIDI, and TQLRAT.

We use the standard notation to represent the high symmetry points in the Brillouin zone. For zinc-blende crystals, these are given by

$$X = (1,0,0),\quad W = (1,0.5,0),\quad L = (0.5,0.5,0.5),\quad \Gamma = (0,0,0),\quad U = K = (0,0.75,0.75) \quad (47)$$

in units of $2\pi/a_0$. For hexagonal crystals, the high symmetry points are defined as

$$\Gamma = (0,0,0),\quad K = (\sqrt{2}/3,\sqrt{2}/3,0),\quad M = (\sqrt{2}/3,0,0),\quad A = (0,0,a_0/\sqrt{2}c_0) = (0,0,\sqrt{3}/4),\quad H = (\sqrt{2/3},\sqrt{2/3},a_0/\sqrt{2}c_0) = (\sqrt{2/3},\sqrt{2/3},\sqrt{3}/4),\quad L = (\sqrt{2/3},0,a_0/\sqrt{2}c_0) = (\sqrt{2/3},0,\sqrt{3}/4) \quad (48)$$

in units of $\sqrt{2}\pi/a_0$. We map bands along these symmetry points to obtain the complete band structure.

V. RESULTS

A. CdS clusters

CdS crystal is a II–VI semiconductor, whose clusters have been extensively investigated experimentally[8–11,14,15,18] and reliable data on their exciton energies are available. These crystals exist in both zinc-blende and hexagonal crystal structures and display similar optical properties in both these lattices.[25,26] This coincidence gives us an opportunity to investigate the effect of crystal structure on the exciton energies in clusters.

We carried out a systematic study of these clusters using the EPM. Figure 1(a) gives the band structure of zinc-blende CdS crystal obtained using this method, $a_0 = 5.818$ Å, and the form factors given in Table I.[25] We diagonalized a 137×137 matrix at a uniformly spaced grid of points in $\mathbf{k}$ space. The energies at each point are converged to about 0.01 eV, which is satisfactory for our purposes. The calculated band gap of 2.44 eV is also in good agreement with the experimental value of 2.5 eV. In addition, this band structure is in qualitative agreement with that obtained using local-density approximation (LDA) and first-principles pseudopotentials.[29] The latter calculations underestimate the band

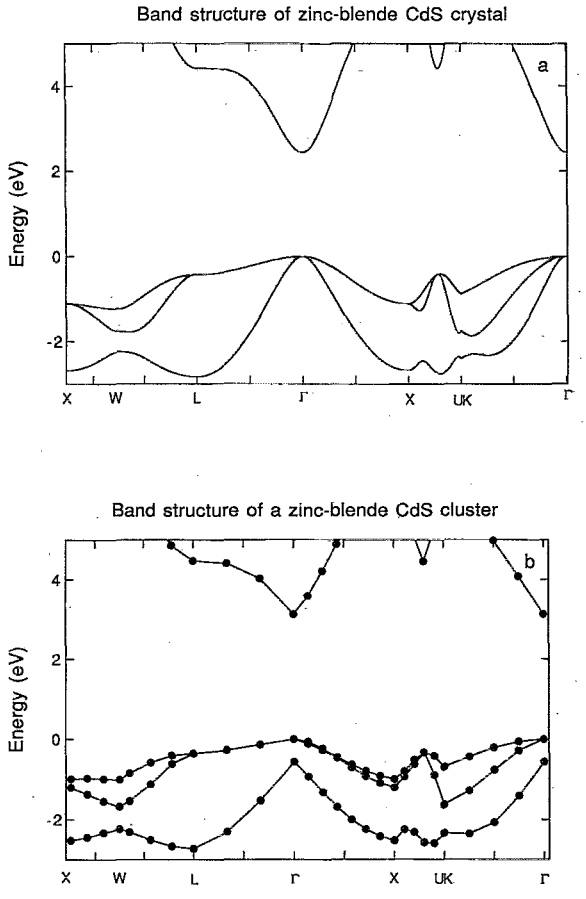

FIG. 1. (a) A portion of the zinc-blende CdS crystal band structure near the top of the valence band. (b) The band structure of a $R = 15$ Å cluster modeled as a sphere.

gap of the crystal by $\approx 30\%$ compared to experiment, because LDA does not describe the conduction bands at the same level of accuracy as the valence bands.[29,30]

The discrete energy levels of a $R = 15$ Å cluster, modeled as a sphere of radius R, are given in Fig. 1(b). The allowed quantum states for this cluster are determined from Eq. (46). We employed 137 **G** vectors to converge the energies of each **k** state to about 0.01 eV. The corresponding band structure for the $R = 15$ Å cluster, modeled as a cube of side length $L = 30$ Å, is very much similar to that given in Fig. 1(b). This is to be expected since Eq. (45) differs from (46) by a small constant factor, the effect of which is to change the location of the eigenstates in the Brillouin zone. Furthermore, for both cubic and spherical models, the top of the valence and the bottom of the conduction bands lie at the smallest **k** given by $(n_x,n_y,n_z) = 1$. For the lowest-energy transition being studied here, only the energy gap at this **k** is of interest. However, knowledge of the complete band structure of the crystal is helpful in visualizing the effect of size and shape on the electronic states in the clusters.

Below, we present the results of our investigation into four different aspects of QCE in CdS clusters: (1) size, (2) crystal structure, (3) physical shape, and (4) lattice constant.

TABLE I. Pseudopotential form factors of CdS, GaAs, and GaP crystals.[a]

Material	G^2	V_S (a.u.)	V_A (a.u.)
CdS (ZB)[b]	0	0.0	0.0
	3	−0.12	0.115
	4	0.0	0.065
	8	0.015	0.0
	11	0.020	0.025
	12	0.0	0.025
CdS (hex)[b]	0	0.0	0.0
	$\frac{3}{4}$	0.0	0.0
	$2\frac{3}{4}$	−0.145	0.0
	3	−0.10	0.115
	$3\frac{5}{12}$	−0.10	0.09
	$5\frac{3}{4}$	−0.012	0.04
	$6\frac{3}{4}$	0.0	0.0
	8	0.015	0.0
	$8\frac{3}{4}$	0.0	0.0
	$9\frac{5}{12}$	0.02	0.025
	$10\frac{3}{4}$	0.02	0.0
	11	0.02	0.025
	$11\frac{5}{12}$	0.02	0.025
	12	0.0	0.025
	$13\frac{3}{4}$	0.01	0.015
	$14\frac{3}{4}$	0.0	0.01
	$14\frac{3}{4}$	0.0	0.0
GaAs[c]	0	0.0	0.0
	3	−0.1225	0.031
	4	0.0	0.0175
	8	−0.0025	0.0
	11	0.0375	0.0015
	12	0.0	0.0
GaP[c]	0	0.0	0.0
	3	−0.1125	0.064
	4	0.0	0.0265
	8	0.012	0.0
	11	0.038	0.01
	12	0.0	0.0

[a] G^2 is the square of the reciprocal-lattice vector, and V_S and V_A are the symmetric and antisymmetric form factors, respectively. For all values of G^2 larger than those given here, V_S and V_A are equal to zero.
[b] Reference 25.
[c] Reference 39.

1. Size effect

From the discrete band structures of clusters we calculated the band gaps (E_g) as a function of the cluster size. We diagonalized a 283×283 matrix for each cluster, to converge E_g to better than 0.01 eV accuracy. Since the EPM underestimates the bulk crystal band gap by 0.06 eV, we add this to the EPM calculated band gaps to obtain E_g. To E_g we added the electron–hole Coulomb and correlation energies to obtain the exciton energies E_x,[9,17]

$$E_x = E_g - \frac{1.786}{\epsilon R} - 0.248 E_{Ry}, \tag{49}$$

where ϵ is the dielectric constant and E_{Ry} is the effective Rydberg energy of the exciton.[17] The bulk crystal parameters used in these calculations are given in Table II. The third term in Eq. (49), which is due to electron–hole correlation, is only about 0.0171 eV and is independent of the cluster radius. Consequently, this term may be omitted, but we

TABLE II. Parameters of CdS, GaAs, and GaP semiconductors.[a]

Material	a_0 (Å)	m_e	m_h	ϵ	R_x (Å)	E_g (eV)
CdS (ZB)	5.818	0.19	0.80	5.5	30	2.50
CdS (hex)	4.136	0.19	0.80	5.5	30	2.50
GaAs	5.654	0.07	0.68	10.9	95	1.48
GaP	5.451	0.10	0.86	9.1	55	2.22(2.78)

[a] a_0 is the lattice constant; m_e and m_h are the effective masses of the electron and hole, respectively, in units of m_0 (free-electron mass); ϵ is the dielectric constant; R_x is the Bohr radius of the exciton; and E_g is the band gap of the bulk crystal. The direct band gap of GaP is given in parentheses. Since the band gap depends on temperature, all our calculations used E_g obtained by taking the average of its values at 0 and 300 K. These data are compiled from Refs. 11, 13, 15, 25, and 38.

retain it for the sake of completeness. The exciton energies thus calculated are presented in Table III and plotted in Fig. 2(a), along with the results from Brus's effective-mass model[9,17] and the experimental data of Wang and Herron.[15]

The x-ray diffraction spectra of Wang and Herron have revealed that the (111) diffraction peak is shifted to smaller angles θ, with decreasing cluster size.[15] This observation indicates that the average lattice constant in small clusters is smaller than that in large clusters and in the bulk. The reduction in the average lattice constant may be calculated from

$$\frac{a_{02}}{a_{01}} = \frac{\sin\theta_1}{\sin\theta_2}, \tag{50}$$

which is derived from the Bragg diffraction condition $n\lambda = 2d\sin\theta$.[31] In Eq. (50), a_{01} and a_{02} are the lattice constants of clusters with radii R_1 and R_2, respectively, and θ_1 and θ_2 are the corresponding Bragg diffraction angles.

From the x-ray diffraction spectra, Wang and Herron determined that $2\theta = 26.9°$, 27.7°, and 28.5° for $R = 15.0$, 7.5, and 5.0 Å clusters, respectively.[15] From Fig. 3 of Ref. 15 we determined that 2θ is 27.3° for the $R = 10.0$ Å cluster. Finally, by interpolating between the above data points we estimated $2\theta = 28.1°$ for the $R = 6.5$ Å cluster. Using these data and Eq. (50), we found that the lattice constants of $R = 10.0$, 7.5, and 6.5 Å clusters are reduced from their bulk values by $\%C = 1.4\%$, 3.0%, and 3.9%, respectively. The $R = 5$ Å cluster is experimentally determined to be a pyramid, but the details of its structure are unknown.[15] Consequently, the exciton energies for this cluster are obtained by extrapolation.

TABLE III. Band gaps and exciton energies of zinc-blende CdS clusters obtained using the lattice constant of the bulk crystal.[a]

R (Å)	k ($2\pi/a_0$)	E_g (eV)	V_C (eV)	E_x (eV)
5.0	0.5818	4.75	−0.93	3.80
6.5	0.4475	4.44	−0.72	3.70
7.5	0.3879	4.23	−0.62	3.59
10.0	0.2909	3.75	−0.47	3.26
15.0	0.1939	3.20	−0.31	2.87
22.5	0.1293	2.85	−0.21	2.63
30.0	0.0970	2.71	−0.15	2.54

[a] R is the radius of the cluster; k is the angular momentum wave vector of the lowest exciton state in units of $2\pi/a_0$; E_g is the band gap; V_C is the Coulomb energy; and E_x is the exciton energy. The exciton energies given in this table are plotted in Fig. 2(a) as open circles.

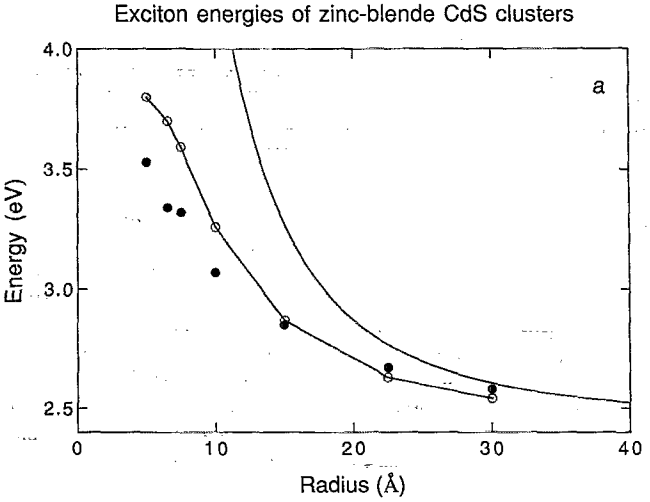

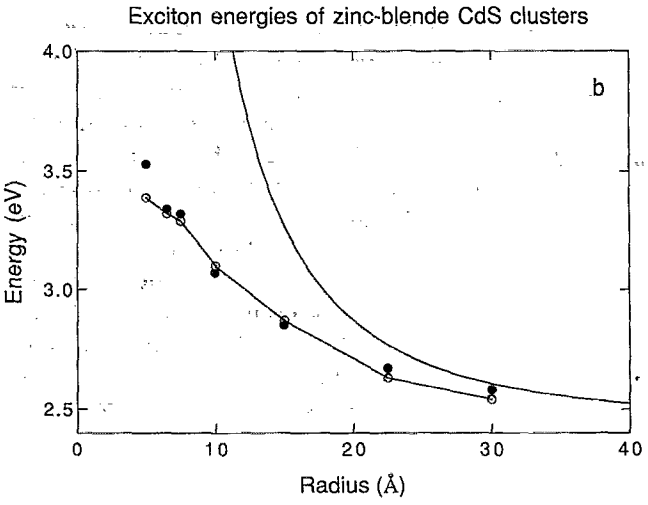

FIG. 2. Experimental and calculated exciton energies of zinc-blende CdS clusters. The solid circles are the experimental data (Ref. 15) and the solid line is the result due to Brus's effective-mass model with $m_e = 0.19$, $m_h = 0.80$, $\epsilon = 5.5$, and $E_g = 2.5$ eV (Refs. 9 and 17). The open circles are calculated (a) using the bulk lattice constant and (b) using the experimentally determined lattice constants for small clusters. These data are tabulated in Tables III and IV.

The exciton energies obtained using the above reduced lattice constants are tabulated in Table IV and plotted in Fig. 2(b). Since these clusters are synthesized in condensed matter, there is no experimental information on the number of CdS molecules (N) present in them. However, we can make an estimate of N using the calculated volumes of the unit cell and the cluster. The volume of the unit cell is a_0^3, the volume of the cluster is $4\pi R^3/3$, and there are four CdS molecules in one conventional unit cell. Hence,

$$N = 16\pi R^3/3a_0^3. \tag{51}$$

For $R = 5.0$, 6.5, 7.5, 10.0, 15.0, 22.5, and 30.0 Å, this formula gives $N = 13$, 26, 39, 89, 287, 969, and 2297, respectively. From Fig. 2(b) and these estimates we clearly see that we are able to reproduce exciton energies reasonably accu-

TABLE IV. Band gaps and exciton energies of zinc-blende CdS clusters obtained using the experimentally determined lattice constants.[a]

R (Å)	k $(2\pi/a_0)$	E_g (eV)	V_C (eV)	E_x (eV)	%C
5.0	0.5585	4.34	−0.93	3.39	4.0
6.5	0.4301	4.06	−0.72	3.32	3.9
7.5	0.3762	3.93	−0.62	3.29	3.0
10.0	0.2868	3.59	−0.47	3.10	1.4
15.0	0.1939	3.20	−0.31	2.87	0.0
22.5	0.1293	2.86	−0.21	2.63	0.0
30.0	0.0970	2.71	−0.15	2.54	0.0

[a] R is the radius of the cluster; k is the angular momentum wave vector of the lowest exciton state in units of $2\pi/a_0$; E_g is the band gap; V_C is the Coulomb energy; E_x is the exciton energy; and %C is the percentage contraction of the lattice constant of the cluster relative to its value in the bulk crystal. The exciton energies given in this table are plotted in Fig. 2(b) as open circles.

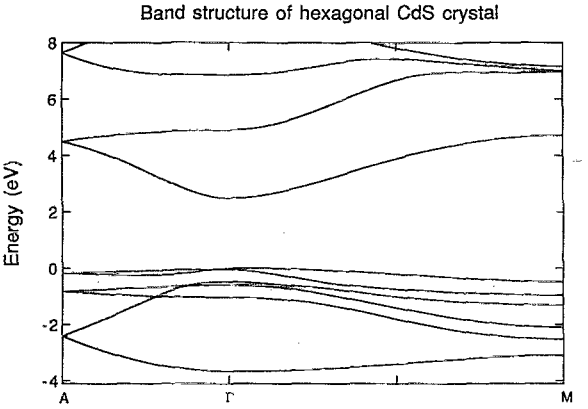

FIG. 3. A portion of the hexagonal CdS crystal band structure near the top of the valence band.

rately for clusters containing as few as 13 CdS monomers. The largest discrepancy is observed for the smallest cluster, because this cluster is not even spherical and the distortion of the lattice is severe. According to experiments, this cluster is a pyramid with a zinc-blende lattice in the interior.[32] Clusters smaller than this size do not have well-defined lattice and our method will fail in these cases. However, it turns out that such very small clusters do not exhibit the characteristic exciton transition of the large clusters and the bulk semiconductor.[33] The calculations of the excited states of such very small clusters would have to be carried out according to the traditional methods of electronic structure theory. Thus, the $R = 5$ Å cluster is, in many ways, at the threshold of a molecule $\Leftrightarrow$ crystal structural transition.

2. Crystal structure effect

The second aspect of the QCE is the effect of crystal structure of the clusters on the exciton energies. To investigate this we repeated the above calculations for clusters with hexagonal symmetry, using $a_0 = 4.136$ Å. At first we used the form factors given in Ref. 25 to calculate the band structure of the crystal. We found that the highest valence band and all the conduction bands are correctly reproduced by these form factors, but discrepancies were observed for the lower bands. Consequently, we adjusted the form factors to improve agreement between our crystal band structure and the published one.[34] With some effort, we found that our band structure improved markedly compared to the published one,[34] if three symmetric form factors are slightly changed.[35] These form factors are given in Table I. The band structure of hexagonal CdS crystal obtained using these new form factors is given in Fig. 3. The calculated band gap is 2.47 eV and the topology of the band structure near the top of the valence band is in agreement with that from LDA first-principles pseudopotential calculation.[29,30]

At first we used the lattice constant of the bulk crystal to calculate the exciton energies of the clusters. These results are given in Table V. Subsequently, we reduced the lattice constants of $R = 10.0$, 7.5, and 6.5 Å clusters by $\%C = 1.4\%$, 3.0%, and 3.9%, respectively, from the bulk crystal value of $a_0 = 4.136$ Å. These percentage reductions in the lattice constants are the same as those used in zinc-blende CdS cluster calculations. The exciton energies thus calculated for a series of clusters are presented in Table VI and Fig. 4. We find that our theoretical results are in agreement with experiment for large clusters, but not for small clusters. This result differs quite dramatically from that of zinc-blende CdS for which both large and small clusters give uniformly good agreement with experiment. This indicates that small CdS clusters are probably zinc-blende type, rather than hexagonal. This prediction is in accord with the experimental data.[15] In addition, our calculations reveal that the band gaps and exciton energies of large clusters with zinc-blende and hexagonal lattices are almost identical to each other. This is not the case for small clusters. These results clearly indicate that the exciton energies in small clusters are sensitive to the crystal structure.

Currently, there are no experimental data on hexagonal CdS clusters with which to compare our theoretical results. This is the first study to address the effect of crystal structure on QCE and future experiments on hexagonal CdS clusters will be helpful.

3. Shape effect

The third aspect of QCE is the sensitivity of the exciton energies to the physical shape of the clusters.[36] The clusters

TABLE V. Band gaps and exciton energies of hexagonal CdS clusters obtained using the lattice constant of the bulk crystal.[a]

R (Å)	k $(\sqrt{2}\pi/a_0)$	E_g (eV)	V_C (eV)	E_x (eV)
5.0	0.5849	5.85	−0.93	4.90
6.5	0.4499	5.07	−0.72	4.33
7.5	0.3899	4.63	−0.62	3.99
10.0	0.2925	3.93	−0.47	3.44
15.0	0.1950	3.24	−0.31	2.91
22.5	0.1300	2.86	−0.21	2.63
30.0	0.0975	2.71	−0.15	2.53

[a] R is the radius of the cluster; k is the angular momentum wave vector of the lowest exciton state in units of $\sqrt{2}\pi/a_0$; E_g is the band gap; V_C is the Coulomb energy; and E_x is the exciton energy.

TABLE VI. Band gaps and exciton energies of hexagonal CdS clusters obtained by gradually decreasing the lattice constants of small clusters according to the percentage contractions of the lattice constants of zinc-blende CdS clusters.[a]

R (Å)	k ($\sqrt{2}\pi/a_0$)	E_g (eV)	V_C (eV)	E_x (eV)	$\%C$
5.0	0.5615	5.61	−0.93	4.66	4.0
6.5	0.4324	4.82	−0.72	4.09	3.9
7.5	0.3782	4.45	−0.62	3.81	3.0
10.0	0.2884	3.82	−0.47	3.33	1.4
15.0	0.1950	3.24	−0.31	2.91	0.0
22.5	0.1300	2.86	−0.21	2.63	0.0
30.0	0.0975	2.71	−0.15	2.53	0.0

[a] R is the radius of the cluster; k is the angular momentum wave vector of the lowest exciton state in units of $\sqrt{2}\pi/a_0$; E_g is the band gap; V_C is the Coulomb energy; E_x is the exciton energy; and $\%C$ is the percentage contraction of the lattice constant of the cluster relative to its value in the bulk crystal. The exciton energies given in this table are plotted in Fig. 4 as open circles.

of interest here, except for the $R = 5$ Å cluster, are experimentally determined to have spherical shapes. Nonetheless, we investigated cubic clusters in order to understand the effect of physical shape on the exciton energies. In Fig. 5 we present these results, along with the exciton energies of spherical CdS clusters and experimental data. From these results we conclude that the shape (cubic vs spherical) has significant effect on the exciton energies even in large clusters. Similar results are obtained for hexagonal CdS clusters also.[37] For zinc-blende CdS clusters, for which experimental data are available, the spherical shape gives better agreement with experiment for all cluster sizes, indicating that these crystallites are approximately spherical. Since we know that

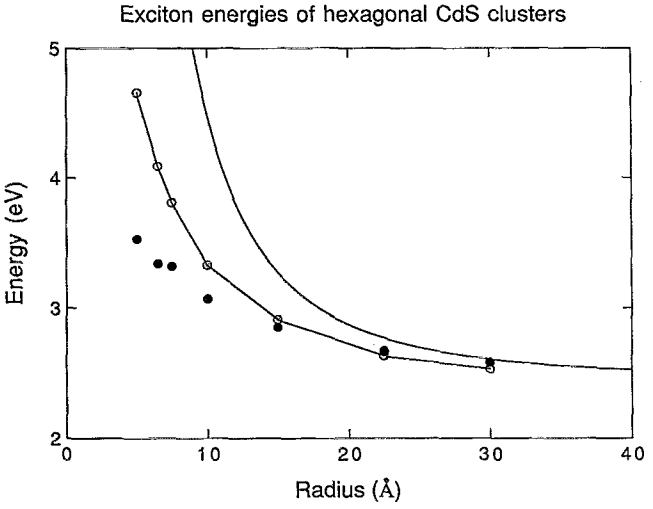

FIG. 4. Exciton energies of hexagonal CdS clusters. The solid circles are the experimental zinc-blende cluster data (Ref. 15) from Fig. 2 and the solid line is the result due to Brus's effective-mass model with $m_e = 0.19$, $m_h = 0.80$, $\epsilon = 5.5$, and $E_g = 2.5$ eV (Refs. 9 and 17). In the absence of experimental data on these clusters, we used the experimentally determined percentage contraction of the lattice constants in zinc-blende clusters to determine the lattice constants of small hexagonal CdS clusters. The exciton energies calculated using these lattice constants are tabulated in Table VI and plotted as open circles in this figure.

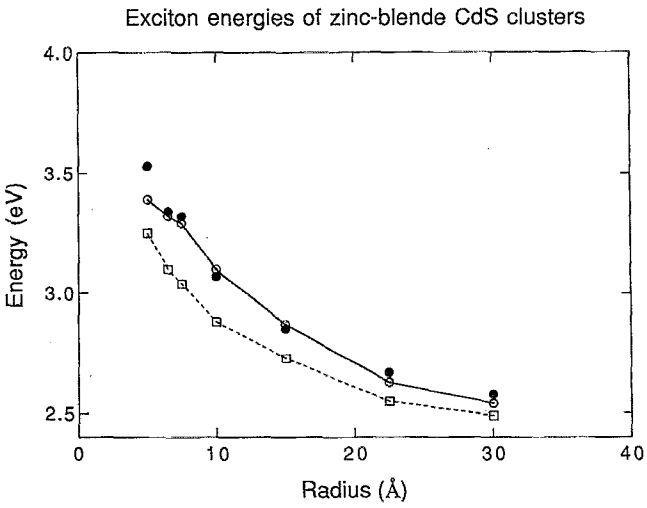

FIG. 5. Exciton energies of zinc-blende CdS clusters. The solid circles are the experimental zinc-blende cluster data (Ref. 15) from Fig. 2. The open squares and open circles are calculated assuming cubic and spherical shapes, respectively, for the clusters.

the kinetic energy of a particle in a box is smaller than that in a sphere of radius $R = L/2$, the cluster exciton energies are underestimated in the cubic clusters, as seen in Fig. 5. The spherical shape increases the kinetic energy just slightly enough to bring the theoretical results into good agreement with experiment. The largest discrepancy between experiment and theory occurs for the $R = 5$ Å cluster. This cluster is a pyramid,[15] but our calculations assumed spherical shape for this cluster also. This explains the observed discrepancy between theory and experiment and confirms that the exciton energies are sensitive to the cluster shape.

Of course, the shape of the cluster would have negligible effect on the exciton energies of very large clusters. The sensitivity to the shape observed in this study indicates that the exciton wave functions have not converged to the bulk limit, even though these clusters have bulk crystal structure.

4. Lattice constant effect

Finally, the fourth aspect of QCE is the sensitivity of the exciton energies to the lattice constant a_0. We found that the exciton energies of $R = 5.0$, 30.0, and ∞ Å zinc-blende clusters are decreased by 0.17, 0.24, and 0.27 eV, respectively, when a_0 is reduced by 0.1 Å. For hexagonal clusters of the same size, the corresponding decrease in the exciton energies are 0.14, 0.32, and 0.35 eV, respectively. These results indicate that the exciton energies of small clusters are less sensitive to a_0 than those of large clusters. This suggests that the curvature of the valence and conduction bands is decreasing as one moves away from the band edges.

B. GaAs clusters

GaAs is an example of a III–V direct-gap semiconductor with zinc-blende lattice structure. Its exciton radius R_x in bulk is 95 Å, which is much larger than the $R_x = 30$ Å for CdS. Because R_x is so large, GaAs clusters are likely to show strong confinement effects and find applications in nonlinear

optical devices.[13] We used the EPM, zinc-blende crystal structure, $a_0 = 5.654$ Å, and the pseudopotentials given in Table I to obtain the band structure of the bulk crystal. This result is plotted in Fig. 6. The band gap of the crystal calculated using the EPM is 1.50 eV, which is 0.02 eV larger than the experimental value of 1.48 eV. The band gaps and exciton energies of the clusters are calculated as outlined in Sec. V A *1*. The calculated band gaps for the clusters are corrected by 0.02 eV to account for the difference in the experimental and theoretical values of the band gap for the bulk crystal.

At first, we calculated the band gaps and exciton energies of clusters by keeping a_0 fixed at its bulk value. These results are presented in Table VII and as open circles in Fig. 7. Subsequently, we decreased a_0 of small clusters gradually such that for $R = 15.0, 10.0, 7.5, 6.5$ Å clusters, a_0 is smaller by $\%C = 0.0\%, 1.5\%, 3.0\%, 4.0\%$, respectively. These results are presented in Table VIII and as the solid circles in Fig. 7. From these results we find that the exciton energies increase (blueshift) first, and then decrease (redshift), with decreasing cluster size. This effect can be explained from Fig. 6. As the cluster size is decreased the k states of highest occupied (HOMO) and the lowest unoccupied (LUMO) molecular orbitals move from Γ toward L. In the case of GaAs the conduction band near Γ is not very deep and there is a turnaround. Consequently, for sufficiently small cluster sizes, the HOMO and LUMO states occur in a region where the conduction-band energies are decreasing with increasing k. At the same time, the valence band is becoming flat. Consequently, the energy difference between the LUMO and HOMO states is decreasing and this gives rise to the redshift observed in the calculations.

Small GaAs clusters have been recently synthesized in polar organic solvents by Olshavsky, Goldstein, and Alivisatos.[13] Using transmission electron microscopy they identified prolate particles with an average major axis of 45 Å and a minor axis of 35 Å. The entire cluster is not crystalline however. Electron-diffraction experiment has revealed that there is a core region within this particle whose radius is 12 Å. The experimentally determined exciton energy for this cluster is 2.52 eV,[13] which is in excellent agreement with our theoretical value of 2.55 eV obtained using the lattice constant of the bulk crystal. If we allow for 0.9% contraction of the lattice constant, then our calculations predict exciton energy to be 2.53 eV. The experimental datum for this cluster is represented in Fig. 7 as an open square. Our theoretical results at least for this cluster are in good agreement with experiment.

TABLE VII. Band gaps and exciton energies of small zinc-blende GaAs clusters obtained using the lattice constant of the bulk crystal.[a]

R (Å)	E_g (eV)	V_C (eV)	E_x (eV)
6.5	2.85	−0.36	2.49
7.5	2.88	−0.31	2.57
10.0	2.85	−0.24	2.61
12.5	2.72	−0.19	2.53

[a] R is the radius of the cluster; V_C is the Coulomb energy; and E_x is the exciton energy. The exciton energies of clusters larger than those given here are tabulated in Table VIII and all these results are plotted in Fig. 7 as open circles connected by a dashed line.

At present there are no experimental data on other GaAs cluster sizes to compare our theoretical predictions with. This paucity in experimental information is due to the difficulties in the controlled synthesis of these clusters.[13]

C. GaP clusters

GaP is a second example of a III–V semiconductor with zinc-blende lattice structure. However, unlike GaAs, the GaP crystal is an indirect-gap semiconductor. In other words, the vertical Franck–Condon transition is not the lowest-energy transition in the absorption spectrum. Instead, the nonvertical, phonon-assisted, transition is the lowest-energy HOMO→LUMO transition in the absorption spectrum. The Franck–Condon transition is allowed because it conserves the momentum of the electron. Consequently, this

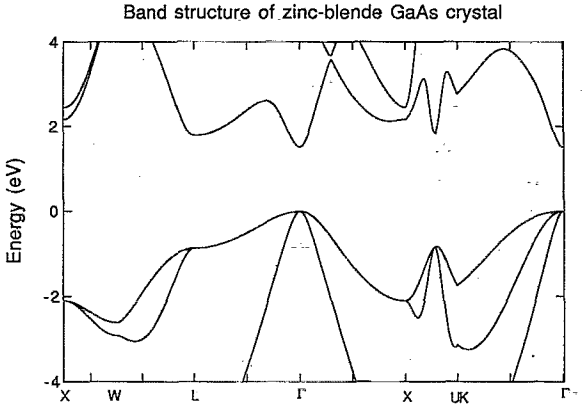

FIG. 6. A portion of the zinc-blende GaAs crystal band structure near the top of the valence band.

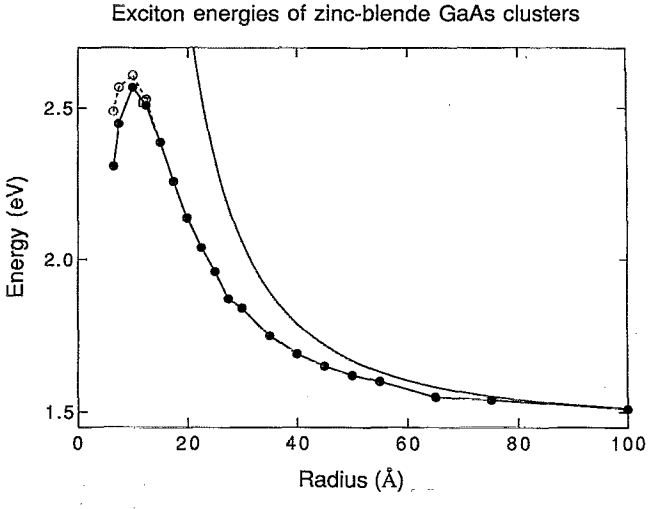

FIG. 7. Exciton energies of GaAs clusters. The solid line is the result due to Brus's effective-mass model with $m_e = 0.07$, $m_h = 0.86$, $\epsilon = 9.1$, and $E_g = 1.48$ eV (Ref. 25). The open circles are calculated assuming bulk lattice constant and the solid circles are calculated assuming small contractions of the lattice constants of small clusters. These data are tabulated in Tables VII and VIII. The lone open square at 12 Å is the experimental datum from Ref. 13.

TABLE VIII. Band gaps and exciton energies of zinc-blende GaAs clusters obtained by gradually decreasing the lattice constants of small clusters.[a]

R (Å)	E_g (eV)	V_c (eV)	E_x (eV)	%C
6.5	2.67	−0.36	2.31	4.0
7.5	2.76	−0.31	2.45	3.0
10.0	2.81	−0.24	2.57	1.5
12.5	2.70	−0.19	2.51	0.75
15.0	2.55	−0.16	2.39	0.0
17.5	2.39	−0.13	2.26	0.0
20.0	2.26	−0.12	2.14	0.0
22.5	2.14	−0.10	2.04	0.0
25.0	2.05	−0.09	1.96	0.0
27.5	1.98	−0.09	1.87	0.0
30.0	1.92	−0.08	1.84	0.0
35.0	1.82	−0.07	1.75	0.0
40.0	1.75	−0.06	1.69	0.0
45.0	1.70	−0.05	1.65	0.0
50.0	1.67	−0.05	1.62	0.0
55.0	1.64	−0.04	1.60	0.0
65.0	1.59	−0.04	1.55	0.0
75.0	1.57	−0.03	1.54	0.0
100.0	1.53	−0.02	1.51	0.0
150.0	1.50	−0.02	1.48	0.0

[a] R is the radius of the cluster; V_C is the Coulomb energy; E_x is the exciton energy; and %C is the percentage contraction of the lattice constant of the cluster relative to its value in the bulk crystal. The exciton energies given in this table are plotted in Fig. 7 as solid circles connected by a solid line.

transition carries most of the transition strength; therefore, it corresponds to the false origin in the spectrum. The real origin of the spectrum corresponds to the non-Franck–Condon transition, which is a higher-order process requiring the absorption or emission of phonons. We investigated the effect of size on these two origins in the spectra of GaP clusters.

We calculated the band structure of GaP crystal using the EPM, zinc-blende lattice structure, $a_0 = 5.451$ Å, and the bulk pseudopotential parameters given in Table I. This result is plotted in Fig. 8. The calculated direct band gap (E_g^d) is 2.79 eV, which is 0.01 eV larger than the experimental value of 2.78. On the other hand, the calculated indirect band gap (E_g^i) of 2.15 eV is 0.07 eV smaller than the experimental value of 2.22 eV. We adjusted the calculated band gaps of clusters by 0.01 and 0.07 eV, respectively, to correctly obtain direct and indirect band gaps.

At first we fixed a_0 at its bulk value and calculated the Franck–Condon and non-Franck–Condon exciton energies of clusters. These results are given in Tables IX and X and as the open circles in Fig. 9, along with the predictions of the EMM. Subsequently, we gradually reduced a_0 of small clusters, such that a_0 of $R = 15.0$, 10.0, 7.5, 6.5 Å clusters are smaller than its bulk crystal value by %$C = 0.0$%, 1.5%, 3.0%, 4.0%, respectively. These results are presented in Tables XI and XII and as solid circles in Fig. 9. These results reveal that the Franck–Condon exciton energies shift to blue first, and then to red, with decreasing cluster size. On the other hand, the non-Franck–Condon exciton energies always shift to blue with decreasing cluster size. Small structure seen in Fig. 9(b) for the non-Franck–Condon transition are an artifact, arising from our arbitrary choice of a_0 in small clusters. The main outcome of these calculations is

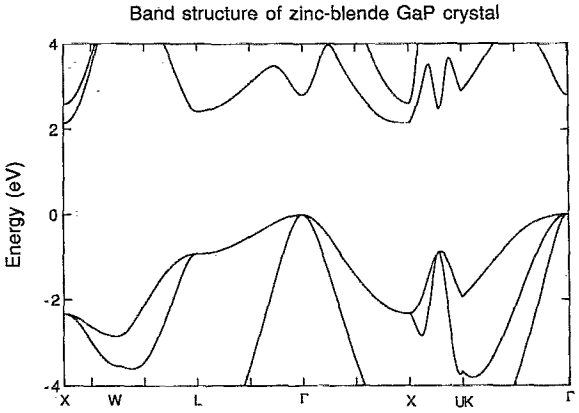

FIG. 8. A portion of the zinc-blende GaP crystal band structure near the top of the valence band.

that the real origin of the absorption spectrum will always shift to blue, whereas the false origin in small clusters will exhibit the anomalous redshift.

VI. PREVIOUS THEORETICAL STUDIES

Ekimov and Onushchenko explained the spectral shift of the absorption spectra of CuCl using the particle in a sphere model.[6] Later, Éfros and Éfros used the EMM to investigate QCE in various confinement regimes.[7] Both these are elementary treatments, because they neglected the Coulomb attraction between the conduction-electron and the valence-band hole. At about the same time, Brus also modeled these clusters using the EMM. His treatment incorporated the Coulomb effects and was able to give qualitatively correct explanation of the observed blueshift of the absorption spectra.[9,11] However, this treatment proved to be quantitatively inadequate, because it overestimated the kinetic energy of the electron and hole. Consequently, Weller and co-workers modified Brus's model by introducing the finite well depth to confine the exciton.[18] This model lowered the kinetic energy of the electron and hole, giving better agreement with experiment for large clusters. For small clusters, even this model was not able to predict the experimental data quantitatively. Subsequently, Kayanuma

TABLE IX. Direct exciton energies of small zinc-blende GaP clusters obtained using the lattice constant of the bulk crystal.[a]

R (Å)	E_g (eV)	V_C (eV)	E_x (eV)
6.5	3.60	−0.43	3.17
7.0	3.63	−0.40	3.23
7.5	3.65	−0.38	3.27
8.0	3.67	−0.35	3.32
9.0	3.70	−0.31	3.39
10.0	3.70	−0.28	3.42
11.0	3.69	−0.26	3.43
12.0	3.66	−0.23	3.43
12.5	3.64	−0.23	3.41

[a] R is the radius of the cluster; E_g is the band gap; V_C is the Coulomb energy; and E_x is the exciton energy. The exciton energies of clusters larger than those given here are tabulated in Table XI and all these results are plotted in Fig. 9(a) as open circles connected by a dashed line.

TABLE X. Indirect exciton energies of small zinc-blende GaP clusters obtained using the lattice constant of the bulk crystal.[a]

R (Å)	E_g (eV)	V_C (eV)	E_x (eV)
6.5	3.44	−0.43	3.01
7.0	3.38	−0.40	2.98
7.5	3.24	−0.38	2.86
8.0	3.14	−0.35	2.79
9.0	3.02	−0.31	2.71
10.0	2.92	−0.28	2.64
11.0	2.83	−0.26	2.57
12.0	2.77	−0.23	2.54
12.5	2.74	−0.23	2.51
20.0	2.50	−0.14	2.36

[a] R is the radius of the cluster; E_g is the band gap; V_C is the Coulomb energy; and E_x is the exciton energy. The exciton energies of clusters larger than those given here are tabulated in Table XII and all these results are plotted in Fig. 9(b) as open circles connected by a dashed line.

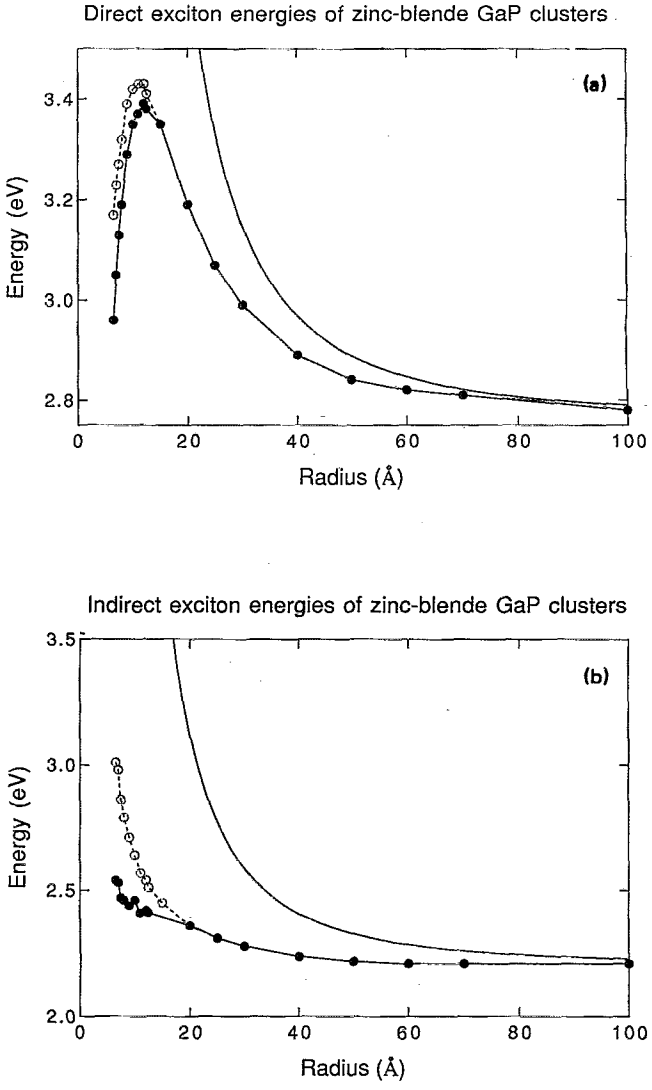

FIG. 9. Direct and indirect exciton energies of GaP clusters. The solid line is the result due to Brus's effective-mass model with $m_e = 0.10$, $m_h = 0.86$, $\epsilon = 9.1$, $E_g^d = 2.78$ eV, and $E_g^i = 2.22$ eV (Refs. 25 and 38). The open circles are calculated assuming bulk lattice constant and the solid circles are calculated assuming small contractions of the lattice constants, as given in Tables IX–XII. (a) gives the direct (Franck–Condon) exciton energies and (b) gives indirect (non-Franck–Condon) exciton energies.

extended the EMM to include electron–hole correlation.[17] This improvisation has only a small effect on the exciton energies and hence did not improve agreement between experiment and theory.

Most recently, Lippens and Lannoo employed an empirical tight-binding Hamiltonian (TBH) to calculate the exciton energies of CdS clusters. These authors took the molecular view, by treating the clusters as large molecules and carrying out electronic structure calculations using a simple basis set. The calculated exciton energies, however, are not in agreement with experiment, except for large cluster sizes.[22] This is because the unoccupied molecular orbitals are not determined as accurately as the occupied molecular orbitals. Furthermore, the TBH tends to emphasize the atomic nature of the cluster, which is not satisfactory for strongly covalently bonded materials. This is particularly so if only the nearest-neighbor interactions are included in the Hamiltonian, as was done in Ref. 22. In principle, an empirical TBH should be able to overcome this deficiency, perhaps when long-range interactions are included in the Hamiltonian. However, the TBH with only nearest-neighbor interactions required diagonalization of $\simeq 10^4 \times 10^4$ matrices.[22] To include the effect of second and more distant neighbor interactions and large basis sets, one would have to diagonalize larger and more dense matrices, which would be computationally prohibitive for large clusters. The EPM overcomes this deficiency by eliminating the core region by use of the pseudopotentials and concentrating on the more important bonding region. Consequently, the results of our calculations are in substantial agreement with experiment. These calculations are also simple to carry out. For example, the largest matrix we diagonalized was only a 427×427 matrix.

Finally, we point out that none of the previous theoretical studies included the effect of the surface on the exciton energies. The main surface effects include lattice relaxation, nonbonding (dangling) orbitals, and surface perturbations. In covalently bonded materials, lattice relaxation gives rise to reduced lattice constants near the surface. On the other hand, nonbonding orbitals give rise to localized electronic states within the band gap. Our calculations included the effect of lattice relaxation by using the experimentally determined reduced lattice constants of the clusters. Computationally, the effect of reduced lattice constants is to modify the matrix elements of the Hamiltonian *via* the kinetic energy and the structure factors. This is the dominant surface effect on exciton energies, in the absence of nonbonding orbitals and other surface perturbations. The nonbonding orbitals are not present in our clusters because the orbitals at the surface of these clusters are saturated (terminated) by neutral organic ligands. Even if some nonbonding orbitals are present, transition strength to these localized states will be small. Likewise, other surface perturbations, such as defects, are either absent in the clusters we model or the energetics of the exciton are not sensitive to such surface perturbations.

TABLE XI. Direct exciton energies of zinc-blende GaP clusters obtained by gradually decreasing the lattice constants of small clusters.[a]

R (Å)	E_g (eV)	V_c (eV)	E_x (eV)	$\%C$
6.5	3.39	−0.43	2.96	4.0
7.0	3.45	−0.40	3.05	3.5
7.5	3.51	−0.38	3.13	3.0
8.0	3.54	−0.35	3.19	2.7
9.0	3.60	−0.31	3.29	2.1
10.0	3.63	−0.28	3.35	1.5
11.0	3.63	−0.26	3.37	1.2
12.0	3.62	−0.23	3.39	0.9
12.5	3.61	−0.23	3.38	0.75
15.0	3.54	−0.19	3.35	0.0
20.0	3.33	−0.14	3.19	0.0
25.0	3.18	−0.11	3.07	0.0
30.0	3.08	−0.09	2.99	0.0
40.0	2.96	−0.07	2.89	0.0
50.0	2.90	−0.06	2.84	0.0
60.0	2.87	−0.05	2.82	0.0
70.0	2.85	−0.04	2.81	0.0
100.0	2.81	−0.03	2.78	0.0

[a] R is the radius of the cluster; E_g is the band gap; V_C is the Coulomb energy; E_x is the exciton energy; and $\%C$ is the percentage contraction of the lattice constant of the cluster relative to its value in the bulk crystal. The exciton energies given in this table are plotted in Fig. 9(a) as solid circles connected by a solid line.

VII. SUMMARY

In this paper we presented the results of our investigations into quantum confinement effects in CdS, GaAs, and GaP clusters. The CdS clusters have been most thoroughly investigated experimentally and there are reliable data to compare our theoretical results with. Furthermore, the bulk CdS crystals exist in both zinc-blende and hexagonal crystal structures, because of which these clusters are ideal for investigating the size-dependent crystal structure effect. The optical spectroscopy of GaAs and GaP clusters is either at a primitive stage or nonexistent at present, and we hope that our theoretical findings will focus experimental attention on these clusters.

We carried out pseudopotential band-structure calculations to investigate all these clusters. The significant findings of this study are as follows.

1. For CdS clusters, our calculations have yielded exciton energies in excellent agreement with experiment over a wide range of cluster sizes.

2. We also found that the shape, crystal structure, and lattice constant of the unit cell all have significant effect on the exciton energies.

3. The exciton energies of small CdS clusters are, in particular, sensitive to whether their crystal structure is zinc blende or hexagonal, even though such a sensitivity is absent in large clusters.

4. The absorption spectra of small GaAs clusters shift to the red, instead of to the blue, with decreasing cluster size.

5. The Franck–Condon transition in small GaP clusters, giving rise to the false origin in the absorption spectrum, exhibits the anomalous redshift with decreasing cluster size. On the other hand, the non-Franck–Condon transition, corresponding to the real origin of the absorption spectrum, does not show this effect.

All these findings, if confirmed by experiments, mean that clusters of different material compositions and crystal structure have widely differing optical properties and that the optical spectroscopy of small semiconductor clusters is dramatically different from those of large clusters and bulk crystals.

TABLE XII. Indirect exciton energies of zinc-blende GaP clusters obtained by gradually decreasing the lattice constants of small clusters.[a]

R (Å)	E_g (eV)	V_C (eV)	E_x (eV)	$\%C$
6.5	2.97	−0.43	2.54	4.0
7.0	2.93	−0.40	2.53	3.5
7.5	2.85	−0.38	2.47	3.0
8.0	2.81	−0.35	2.46	2.7
9.0	2.75	−0.31	2.44	2.1
10.0	2.74	−0.28	2.46	1.5
11.0	2.67	−0.26	2.41	1.2
12.0	2.65	−0.23	2.42	0.9
12.5	2.64	−0.23	2.41	0.75
20.0	2.50	−0.14	2.36	0.0
25.0	2.42	−0.11	2.31	0.0
30.0	2.37	−0.09	2.28	0.0
40.0	2.31	−0.07	2.24	0.0
50.0	2.28	−0.06	2.22	0.0
60.0	2.26	−0.05	2.21	0.0
70.0	2.25	−0.04	2.21	0.0
100.0	2.24	−0.03	2.21	0.0

[a] R is the radius of the cluster; E_g is the band gap; V_C is the Coulomb energy; E_x is the exciton energy; and $\%C$ is the percentage contraction of the lattice constant of the cluster relative to its value in the bulk crystal. The exciton energies given in this table are plotted in Fig. 9(b) as solid circles connected by a solid line.

ACKNOWLEDGMENTS

This is the third paper in this series on semiconductor clusters. All the calculations reported here were carried out on the Cray Y-MP supercomputer at the Pittsburgh Supercomputing Center and IBM RISC 6000/320 POWERstation. This work is supported by the Department of Energy (Grant No. DE-FG-02-90-ER14162). Finally, one of us (R.K.) is grateful to Y. Wang for thoughtful discussions and for communicating the beautiful experimental data of Fig. 2 in Ref. 15.

[1] E. Corcoran, *Diminishing Dimensions*, Sci. Am. **263** (November), 122 (1990).

[2] W. D. Knight, K. Clemenger, W. A. de Heer, W. A. Saunders, M. Y. Chou, and M. L. Cohen, Phys. Rev. Lett. **52**, 2141 (1984); H. Göhlich, T. Lange, T. Bergmann, and T. P. Martin, *ibid.* **65**, 748 (1990); S. Bjornholm, J. Borggreen, O. Echt, K. Hansen, J. Pedersen, and H. D. Rasmussen, *ibid.* **65**, 1627 (1990).

[3] M. V. Rama Krishna and K. B. Whaley, Phys. Rev. Lett. **64**, 1126 (1990); J. Chem. Phys. **93**, 746 (1990); **93**, 6738 (1990); Mod. Phys. Lett. B **4**, 895 (1990); Z. Phys. D **20**, 223 (1991); Phys. Rev. B **38**, 11 839 (1988).

[4] S. Bjornholm, Contemp. Phys. **31**, 309 (1990).

[5] D. Snoke, J. P. Wolfe, and A. Mysyrowicz, Phys. Rev. Lett. **59**, 827 (1987); Y. Z. Hu, S. W. Koch, M. Lindberg, N. Peyghambarian, E. L. Pollock, and F. F. Abraham, *ibid.* **64**, 1805 (1990); Y. Z. Hu, S. W. Koch, and D. B. T. Thoai, Mod. Phys. Lett. B **4**, 1009 (1990); L. Wang, L. P. F. Chibante, F. K. Tittel, R. F. Curl, and R. E. Smalley, Chem. Phys. Lett. **172**, 335 (1990).

[6] A. I. Ekimov and A. A. Onushchenko, *Pis'ma Zh. Eksp. Teor. Fiz.* **34**, 363

(1981) [JETP Lett. **34**, 345 (1981)]; Fiz. Tekh. Poluprovodn. **16**, 1215 (1982) [Sov. Phys. Semicond. **16**, 775 (1982)].
[7] Al. L. Éfros and A. L. Éfros, Fiz. Tekh. Poluprovodn. **16**, 1209 (1982) [Sov. Phys. Semicond. **16**, 772 (1982)].
[8] R. Rosetti and L. E. Brus, J. Phys. Chem. **86**, 4470 (1982).
[9] L. E. Brus, J. Phys. Chem. **90**, 2555 (1986); M. L. Steigerwald and L. E. Brus, Acc. Chem. Res. **23**, 183 (1990); M. G. Bawendi, M. L. Steigerwald, and L. E. Brus, Annu. Rev. Phys. Chem. **41**, 477 (1990).
[10] R. Rosetti, S. Nakahara, and L. E. Brus, J. Chem. Phys. **79**, 1086 (1983).
[11] L. E. Brus, J. Chem. Phys. **79**, 5566 (1983); **80**, 4403 (1984).
[12] M. G. Bawendi, A. R. Kortan, M. L. Steigerwald, and L. E. Brus, J. Chem. Phys. **91**, 7282 (1989); M. G. Bawendi, W. L. Wilson, L. Rothberg, P. J. Carroll, T. M. Jedju, M. L. Steigerwald, and L. E. Brus, Phys. Rev. Lett. **65**, 1623 (1990); J. J. Shiang, A. N. Goldstein, and A. P. Alivisatos, J. Chem. Phys. **92**, 3232 (1990); V. L. Colvin, A. P. Alivisatos, and J. G. Tobin, Phys. Rev. Lett. **66**, 2786 (1991).
[13] M. A. Olshavsky, A. N. Goldstein, and A. P. Alivisatos, J. Am. Chem. Soc. **112**, 9438 (1990).
[14] Y. Wang, A. Suna, W. Mahler, and R. Kasowsky, J. Chem. Phys. **87**, 7315 (1987); Y. Wang, J. Phys. Chem. **95**, 1119 (1991).
[15] Y. Wang and N. Herron, Phys. Rev. B **42**, 7253 (1990).
[16] Y. Kayanuma, Solid State Commun. **59**, 405 (1986).
[17] Y. Kayanuma, Phys. Rev. B **38**, 9797 (1988).
[18] H. Weller, H. M. Schmidt, U. Koch, A. Fojtik, S. Baral, A. Henglein, W. Kunath, K. Weiss, and E. Dieman, Chem. Phys. Lett. **124**, 557 (1986).
[19] P. V. Kamat, K. R. Gopidas, and D. Weir, Chem. Phys. Lett. **149**, 491 (1988); K. R. Gopidas and P. V. Kamat, J. Phys. Chem. **93**, 6428 (1989); Langmuir **5**, 22 (1989); Mater. Lett. **9**, 372 (1990); K. R. Gopidas, M. Boborquez, and P. V. Kamat, J. Phys. Chem. **94**, 6435 (1990); P. V. Kamat and K. R. Gopidas, SPIE Proc. **1209**, 115 (1990); H. M. Schmidt and H. Weller, Chem. Phys. Lett. **129**, 615 (1986); S. V. Nair, S. Sinha, and K. C. Rustagi, Phys. Rev. B **35**, 4098 (1987).
[20] T. Takagahara, Phys. Rev. B **36**, 9293 (1987); **39**, 10 206 (1989).
[21] E. Hanamura, Phys. Rev. B **37**, 1273 (1988).
[22] P. E. Lippens and M. Lannoo, Phys. Rev. B **39**, 10 935 (1989).
[23] H. Haken, *Quantum Field Theory of Solids* (North-Holland, Amsterdam, 1976), Chap. 4.
[24] D. Brust, J. C. Phillips, and F. Bassani, Phys. Rev. Lett. **9**, 94 (1962); D. Brust, in *Methods in Computational Physics*, edited by B. J. Alder, S. Fernbach, and M. Rotenberg (Academic, New York, 1968), Vol. 8.
[25] T. K. Bergstresser and M. L. Cohen, Phys. Rev. **164**, 1069 (1967); M. L. Cohen and J. R. Chelikowsky, *Electronic Structure and Optical Properties of Semiconductors* (Springer, Berlin, 1989).
[26] H. J. Emeléus and A. G. Sharpe, *Modern Aspects of Inorganic Chemistry*, 4th ed. (Routledge and Kagan Paul, London, 1973), p. 53.
[27] R. W. G. Wyckoff, *Crystal Structures* (Interscience, New York, 1963), pp. 108 and 111.
[28] S. Flügge, *Practical Quantum Mechanics* (Springer, Berlin, 1971).
[29] K. J. Chang, S. Froyen, and M. L. Cohen, Phys. Rev. B **28**, 4736 (1983).
[30] C. S. Wang and B. M. Klein, Phys. Rev. B **24**, 3393 (1981).
[31] C. Kittel, *Introduction to Solid State Physics*, 6th ed. (Wiley, New York, 1986).
[32] Y. Wang (private communication).
[33] Y. Wang and N. Herron, J. Phys. Chem. **95**, 525 (1991), Fig. 3.
[34] A. Kobayashi, O. F. Sankey, S. M. Volz, and J. D. Dow, Phys. Rev. B **28**, 935 (1983).
[35] We used $V_S(\sqrt{8/3}) = -0.145$, $V_S(\sqrt{3}) = -0.10$, and $V_S(\sqrt{17/3}) = -0.012$ a.u. instead of -0.13, -0.12, and -0.015 a.u., respectively, given in Ref. 25. All other form factors are identical to those in Ref. 25. The cluster calculations were carried out without any additional changes.
[36] V. Mohan and J. B. Anderson, Chem. Phys. Lett. **156**, 520 (1989).
[37] M. V. Rama Krishna and R. A. Friesner, Phys. Rev. Lett. **67**, 629 (1991); SPIE Proc. **1599** (1991).
[38] C. V. de Alvarez, J. P. Walter, M. L. Cohen, J. Stokes, and Y. R. Shen, Phys. Rev. B **6**, 1412 (1972).
[39] J. P. Walter and M. L. Cohen, Phys. Rev. **183**, 763 (1969).